FULL LENGTH	Iranian Biomedical Journal 29 (6): 437-450 November 2025

Novel *FKBP10* Mutation in Iranian Patients with Osteogenesis Imperfecta: Insights from Whole-Exome Sequencing to Molecular Dynamics

Moslem Hoseinbeyki[1], Shirin Moradifard[1], Fatemeh Mirkhani[1], Fatemeh Sadat Shariati[1], Parastoo Ehsani[2], Mohammad Reza Alaei[3*], Mina Ebrahimi-Rad[1*]

[1]Biochemistry Department, Pasteur Institute of Iran, Tehran, Iran; [2]Molecular Biology Department, Pasteur Institute of Iran, Tehran, Iran; [3]Department of Pediatric Endocrinology and Metabolism, Mofid Children's Hospital, Shahid Beheshti University of Medical Sciences, Tehran, Iran

OPEN ACCESS

Article type: Research Article
Received: August 10, 2025
Revised: September 12, 2025
Accepted: September 18, 2025
Published online: September 20, 2025

How to cite:
Hoseinbeyki M, Moradifard S, Mirkhani F, Shariati FS, Ehsani P, Alaei MR, Ebrahimi-Rad M. Novel *FKBP10* Mutation in Iranian Patients with Osteogenesis Imperfecta: Insights from Whole-Exome Sequencing to Molecular Dynamics. *Iran. Biomed. J.* 2025; 29(6): 437-450.

ABSTRACT

Background: Osteogenesis imperfecta is a rare hereditary disorder affecting bone and connective tissue. While most cases are linked to autosomal dominant mutations in the *COL1A1* and *COL1A2* genes, *FKBP10* variants are associated with the autosomal recessive form of OI, type XI. The study represents the first cohort-based evaluation of the *FKBP10* mutational spectrum in Iranian patients, leading to the discovery of a novel variant.

Methods: Thirty Iranian patients clinically diagnosed with OI were enrolled for genetic analysis. WES was performed to identify pathogenic variants, validated by PCR and sanger sequencing in patients and their parents. To explore the biological relevance of the identified variants, we constructed PPI networks and performed functional enrichment analysis using the ClueGO plugin. MD simulations with GROMACS were used to assess the structural impact of the mutations.

Results: Among 30 families, four exhibited pathogenic *FKBP10* variants. Three patients were homozygous for the previously reported mutation (*c.831dupC*: *p. G278Rfs95*), while the fourth harbored a novel homozygous deletion (*c.855_859del: p. G286Lfs84*). Network analysis revealed significant involvement of *CRTAP, IFITM5, SERPINF1, PPIB, FKBP10, P3H1, SERPINH1,* and *PLOD2* in collagen-related pathways. Computational modeling and MD simulations indicated reduced flexibility and more compact folding in the mutant FKBP10 protein, which aligns with impaired protein function and defective collagen processing.

Conclusion: This study reports a novel *FKBP10* variant and presents the first cohort-based analysis of *FKBP10* mutations in Iranian patients with OI. It demonstrates the value of combining WES with computational modeling to elucidate the molecular mechanisms underlying OI. ***DOI: 10.61882/ibj.5278***

Keywords: FKBP10 protein, Frameshift mutation, Exome sequencing, Osteogenesis imperfecta

Corresponding Authors:
Mohammad Reza Alaei
Department of Pediatric Endocrinology and Metabolism, Mofid Children's Hospital, Shahid Beheshti University of Medical Sciences, Tehran, Iran; Tel.: (+98-912) 1884972; E-mail: Alaee2003@yahoo.com; ORCID ID: 0000-0002-9920-9431

Mina Ebrahimi-Rad
Biochemistry Department, Pasteur Institute of Iran, Tehran, Iran; Tel.: (+98-21) 64112170; Fax: (+98-21) 64112100; E-mail: minebrad@pasteur.ac.ir; ORCID ID: 0000-0002-4208-2206

List of abbreviations
MD: molecular dynamics; **OI:** osteogenesis imperfect; **PPI:** protein-protein interaction; **PTM:** post-translational modification; **RMSD:** root mean-square deviation; **RMSF:** root mean-square fluctuation; **WES:** Whole-exome sequencing

[DOI: 10.61882/ibj.5278]

INTRODUCTION

Osteogenesis imperfecta is a rare genetic disease characterized by low bone mass, increased bone fragility, skeletal deformities, growth deficiency, and less frequent extra-skeletal symptoms, such as hearing impairment, bluish sclera, joint laxity, and dentinogenesis imperfecta[1]. The incidence of OI is estimated to be approximately 1 in 15,000 to 20,000 live births. However, due to its broad phenotypic spectrum, this disorder is likely underdiagnosed[2]. The prevalence of OI in the Iranian population has not yet been determined. The initial clinical classification of OI was proposed by Sillence et al. in 1979. They categorized the disorder into four distinct types based on phenotypic severity and radiographic features: Type I (Mendelian Inheritance in Man [MIM] 166200), Type II (MIM 166210), Type III (MIM 259420), and Type IV (MIM 166220)[3]. Over time, this classification has been expanded to include more than 20 OI types genetically distinct. Clinically, Type 1 is the most common form of OI, characterized by a milder phenotype than other types[4]. Approximately 85-90% of OI cases are attributed to dominant mutations in *COL1A1* and *COL1A2* genes, which encode type I collagen. These variants disrupt collagen synthesis, secretion, and triple helix formation, ultimately impairing structural stability and increasing bone fragility[4].

The first gene identified in association with autosomal recessive OI was *CRTAP* (IM 605497)[5]. Subsequently, mutations in *LEPRE1*, *PPIB*, *PLOD2*, *IFITM5*, and *FKBP10* were reported as additional causes of recessive forms of OI[5]. These genes are involved in PTM, folding, cross-linking, and trafficking of collagen[6]. Among the mentioned genes, *FKBP10* encodes a 65-kDa protein, first identified by Patterson and colleagues[7]. FKBP 65 (FK506-binding protein 65) is a molecular chaperone localized to the rough endoplasmic reticulum. It exhibits peptidyl-prolyl cis–trans isomerase (PPIase) activity and interacts with type I collagen and tropoelastin, facilitating proper collagen folding and cross-linking. Mutations in *FKBP65* may affect the secretion of type I collagen[8]. Thus, in addition to the defects leading to alterations in the structure, synthesis, and PTM of type I procollagen, the loss of *FKBP10* chaperone activity can produce a progressive and deforming OI phenotype[9]. Besides OI type XI caused by *FKBP10* mutations, Bruck syndrome (MIM 259450 and 609220)—characterized by congenital joint contractures and bone fragility—may also result from mutations in *FKBP10* and *PLOD2* (types 1 and 2, respectively)[5,10]. Alanay et al. identified homozygous *FKBP10* mutations in a Turkish population with OI and Bruck syndrome, indicating *FKBP10* critical role in maintaining skeletal integrity[11]. In another study of a different population, *FKBP10* variants were examined in Russian families to address clinical similarities between Bruck syndrome and recessive OI type XI[12]. Furthermore, the study by Alfares et al. provided evidence for the effectiveness of WES in identifying *FKBP10* variants in consanguineous Saudi families[13]. Essawi et al. also demonstrated phenotypic variability in recessive OI caused by *FKBP10* mutations through genotype-phenotype correlation[14].

Despite numerous reports of *FKBP10*-related OI variants in diverse populations, including South Africa[15], Russia[12], Saudi Arabia[13,16], and Palestine[14], a significant proportion of OI cases remain unidentified in specific populations, such as Iran. A previous case report from Iran described a single *FKBP10* mutation in an individual with OI[17], but no cohort-based investigation of *FKBP10*-related OI has been conducted among Iranian patients.

WES is a valuable tool for detecting mutations in coding regions of the genome, and advances in this technology have facilitated the discovery of novel genes and pathogenic variants in OI[18]. Moreover, computational modeling and MD simulations are powerful in silico approaches for examining protein structure, dynamics, flexibility, and stability. However, existing studies have primarily focused on genetic identification and phenotypic description, with no published data on MD analyses of *FKBP10*-coded proteins, either wild-type or mutant. This limitation indicates a significant knowledge gap in understanding the molecular mechanisms linking *FKBP65* dysfunction to OI[19].

In this study, 30 Iranian patients clinically diagnosed with OI were investigated using WES. We identified a novel, previously unreported homozygous deletion variant in *FKBP10*, along with an additional frameshift mutation. In addition to mutational scanning, we performed computational modeling and MD simulations using GROMACS to investigate the stability and conformational changes of mutants versus the wild-type protein, providing the first structural analysis of *FKBP10* mutants. These combined approaches enabled us to link patients' genotype-phenotype correlations with in silico predictions of the functions of *FKBP10* mutant proteins relative to the wild-type, providing mechanistic insights into disease pathology. In another step of our work, a PPI network for *FKBP10* was constructed using the STRING database, and functional enrichment analysis was performed with the ClueGO plugin. To date, no cohort studies have reported *FKBP10* mutations in Iran, and no structural or MD studies of *FKBP10* in OI have been published worldwide. The current study was designed to address these gaps.

[DOI: 10.61882/ibj.5278]

MATERIALS AND METHODS

Patient recruitment and clinical evaluation

Thirty independent Iranian families whose siblings were affected by OI were clinically diagnosed by pediatric endocrinologists. They were referred to the Biochemistry Department of the Pasteur Institute of Iran and enrolled in the study. A structured questionnaire was used to collect demographic data, clinical history, and fracture records. All patients had experienced multiple fractures resulting from minimal or no trauma. The patients with identified *FKBP10* mutations, who were the subjects of the current study, included one male (3.3 years) and three females (aged 15.4, 9.4, and 9.7 years). Based on the Sillence classification, patients 1 and 3 were diagnosed with OI Type IV and patient 2 with Type III; however, the clinical type of patient 4 remained undetermined. Detailed clinical characteristics of the patients are summarized in Table 1.

Blood collection and DNA extraction

Peripheral blood samples (4 mL) were collected from each patient and their parents into EDTA-containing tubes. Genomic DNA was extracted using the blood DNA extraction kit (Gene Transfer Pioneers, Iran, cat. no: DB10025, DB10050, DB10100) following the manufacturer's protocol. DNA concentration and purity were assessed using NanoDrop spectrophotometry at 260/280 nm. Additionally, to assess the integrity of the extracted DNA, 2 µL of genomic DNA was subjected to gel electrophoresis.

Whole-exome sequencing

WES was performed to identify pathogenic genes and mutations related to OI in the studied patients. Following DNA extraction from patients' peripheral blood, samples were sent to BGI Genomics (China) for sequencing. Using the BGISEQ-500 (China), WES was conducted to sequence all protein-coding genes

Table 1. Clinical and demographic characteristics of patients with OI harboring *FKBP10* mutations

Parameter	Patient 1	Patient 2	Patient 3	Patient 4
Gender	M	F	F	F
Age (y/m)	3.6	15.4	9.4	9.7
Weight (kg)	12.5	28	21.7	32
Height(m)	0.85	1.2	1.12	1.32
Weight (Z score)	-1.91	-2.2	-2.29	-0.3
Height (Z score)	-3.64	-3.8	-3.91	-1.2
BMI (Kg/m^2)	17.30104	19.44444	17.29911	18.36547
Clinical type	IV	III	IV	UN
Consanguinity	Yes	Yes	Yes	Yes
Positive family history	No	No	Yes	No
First fracture (year)	8 days	2	0.3	0.9
Last fracture	2.6	14.1	8.11	8.11
Intrauterine fractures	No	No	No	No
perinatal fractures	No	No	No	No
Fracture (number)	8	30	8	10
Fracture/age	2.222222	1.948052	0.851064	1.030928
Surgery (number)	0	6	4	3
Teeth problems	-	-	Yes	Yes
Dentinogenesis imperfecta	Yes	No	No	No
Hearing loss	No	No	No	No
Scoliosis/kyphoscoliosis	No	Yes	No	No
Triangular fancies	No	Yes	Yes	No
thoracic cage deformity	Yes	Yes	Yes	Yes
Rhizomelia	UN	UN	UN	UN

Clinical classification was based on the Silence criteria (Types III–IV). Z-scores for weight, height, and BMI were determined relative to age- and sex-matched population norms. Clinical variables included fracture history (first, last, total number, and rate per year of age), presence of dentinogenesis imperfecta, scoliosis/kyphoscoliosis, thoracic cage deformity, triangular facies, and other skeletal or extra skeletal findings. Consanguinity and family history were recorded to reflect pedigree information. M: male; F: female; UN: undetermined

[DOI: 10.61882/ibj.5278]

(exomes) and other critical genomic regions according to the manufacturer's protocol. The BGISEQ-500, first introduced by BGI Genomics as a sequencer in October 2015, employs library construction and combined primer anchor synthesis technologies derived from Complete Genomics™ sequencing and utilizes DNA NanoBalls[20]. Raw sequencing reads were aligned to the human reference genome (hg19/GRCh37) using the Burrows-Wheeler Aligner tool[21] to generate Binary Alignment Map files. Variant calling was subsequently performed using the Genome Analysis Toolkit[22] in accordance with best-practice recommendations, including base quality score recalibration and variant filtration. Identified variants were then annotated using ANNOVAR to obtain gene-based, region-based, and functional information. For variant filtering, common variants with a minor allele frequency >1% in population databases such as gnomAD[23], 1000 Genomes[24], and ExAC[25] were excluded. Only high-quality variants with a read depth ≥10 and genotype quality ≥20 were retained. Nonsynonymous, frameshift, splice-site, stop-gain, and stop-loss variants were prioritized for further analysis. Variants predicted to be deleterious by multiple in silico tools (e.g., SIFT, PolyPhen-2, CADD, REVEL) and consistent with the disorder inheritance model were selected for interpretation. Public databases, including ClinVar, OMIM, and dbSNP, were consulted to assess the clinical significance of the identified variants.

PCR amplification

Based on WES results, primers targeting exon 5 of the *FKBP10* gene were designed using Oligo7 and NCBI Primer-BLAST. Primer sequences were as follows: forward: 5'-AAAGGGCTCTGGAGAGTGG-3' and reverse: 5'-CACAATGGGCAGTTCGGAG-3'. Targeted PCR was performed on the DNA of patients and their parents in a 50 µL reaction containing 2 µg of template DNA, 2 ng of each primer, 25 µL of 2× SinaClon PCR Master Mix (Tehran, Iran; Cat. No. MM2011), and 19 µL of double-distilled water. Thermal cycling conditions included an initial denaturation at 95 °C for 5 min, followed by 35 cycles of 95 °C for 45 s, 59 °C for 45 s, 72 °C for 45 s, and a final extension at 72 °C for 10 min.

Sanger sequencing

To validate WES findings (detected mutations) and assess inheritance patterns, bidirectional sanger sequencing was performed on PCR products from patients and their parents using an ABI sequencer and a commercial sanger sequencing kit (ABI BIGdye v3.1, Thermo Fisher Scientific, USA). Sequencing data were analyzed using Chromas v2.6.5 (http://www.technelysium.com.au/chromas.html) and NCBI BLAST for alignment and variant confirmation.

PPI and functional analysis

The PPI network for *FKBP10* was constructed using the STRING v. 11.5 database, with a medium confidence cutoff of 0.4[26]. The resulting network, comprising 11 nodes, was then imported into Cytoscape 3.9.1 for further analysis, visualization, and functional enrichment[27]. To analyze the ontology and pathway network for 11 proteins, we used the ClueGO v. 2.5.8 plugin in Cytoscape 3.9.1[26,28]. In ClueGO (v. 2.5.8). functional enrichment was performed using a two-sided hypergeometric test with Bonferroni step-down correction for *p*-value adjustment to link GO/pathways to functionally grouped networks. Gene ontology and pathway enrichment analyses were performed, using a Kappa score of 0.4 to define GO/pathway similarity based on shared genes.

In silico studies of the *FKBP10* mutant proteins

Since the crystal structure of the FKBP10 protein is not available in the PDB databases, we used three popular tools, Swiss-Model, Modeller, and AlphaFold, to generate homology models of the FKBP10 protein. The amino acid sequence corresponding to UniProt (www.UniProt.org; accession ID Q96AY3) was retrieved and used as input for homology modeling. For the Swiss-Model, we used the default settings, and the closest template was selected based on the highest identity score[29]. Moreover, the Modeller and AlphaFold were run with the standard parameters and default settings, respectively. The lowest (the most negative) DOPE score was used to select the best model from Modeller[30], while the AlphaFold model was assessed using intrinsic confidence metrics, including pLDDT scores and PAE plots. To facilitate a unified comparison among Swiss-Model, MODELLER, and AlphaFold models, we evaluated all final structures using PROCHECK and Ramachandran plot analysis, which provide information on amino acid distribution in protein structures and identify potential errors[30]. Schrodinger software was subsequently used to create mutations in the protein structure. In Mutant 1 of FKBP10, glycine at residue 286 was converted to leucine, and in mutant 2, glycine at residue 278 was substituted by arginine. Notably, the variants p. G278Rfs*95 and p. G286Lfs*84 were modeled as frameshift mutations based on their cDNA-level alterations (c.831dupC and c.855_859del), which change the downstream reading frame and introduce premature stop codons. Thus, truncated mutant protein sequences (<400 amino acids) were used for modeling and MD simulations rather than single-residue substitutions. Energy minimization was finally performed to relax the structure and ensure that the mutations did not compromise protein stability.

[DOI: 10.61882/ibj.5278]

Domain architecture analysis

Domain architecture analysis of wild-type and mutant FKBP10 proteins was performed using InterProScan to evaluate the functional impact of mutations in the conserved domains[31]. The FKBP10 protein sequence (accession number Q96AY3) was extracted from UniProt and analyzed using InterProScan software, which identified domain positions and visualized losses due to frameshifts or truncations.

MD simulation

MD simulations were performed with GROMACS version 2021.2 at 310 K and 1.0 bar. The initial protein structures were prepared using the Amber 99SB force field and TIP3P water molecules, with the system solvated in a triclinic water box, leaving at least 1.0 nm between the protein surface and the box boundaries to ensure proper solvation. To neutralize the system and adjust the physiological ionic strength to 0.15 M, we added sodium and chloride ions to the simulation box. System sizes and box dimensions varied based on protein length: wild-type FKBP10 contained 824,901 atoms in a 20.45 × 20.45 × 20.16 nm³ box; p.G278Rfs95 had 294,153 atoms in a 14.41 × 14.41 × 14.45 nm³ box; p.G286Lfs84 had 269,001 atoms in a 13.16 × 13.16 × 15.86 nm³ box[19,32]. Energy minimization was carried out before equilibration, which was performed in two phases: (1) 1 nanosecond (ns) under constant volume and temperature (NVT ensemble) using the Nose–Hoover thermostat, followed by (2) 1 ns constant pressure and temperature (NPT ensemble) using the Berenson barostat[33]. Long-range electrostatic interactions were computed using the Particle Mesh Ewald method. At the same time, van der Waals forces were applied using the Lennard-Jones potential within a cutoff distance of 1 nm. Bond constraints were applied using the LINCS algorithm[34]. A 100-ns production MD simulation was performed, and atomic coordinates were recorded every 10 picoseconds for subsequent analysis.

RESULTS

WES and clinical findings

In this study, 30 Iranian patients clinically diagnosed with OI were investigated. WES revealed that four patients with clinically normal consanguineous parents harbored mutations in the *FKBP10* gene (Fig. 1). Patients 1, 2, and 4 were homozygous for a previously reported frameshift insertion in *FKBP10*

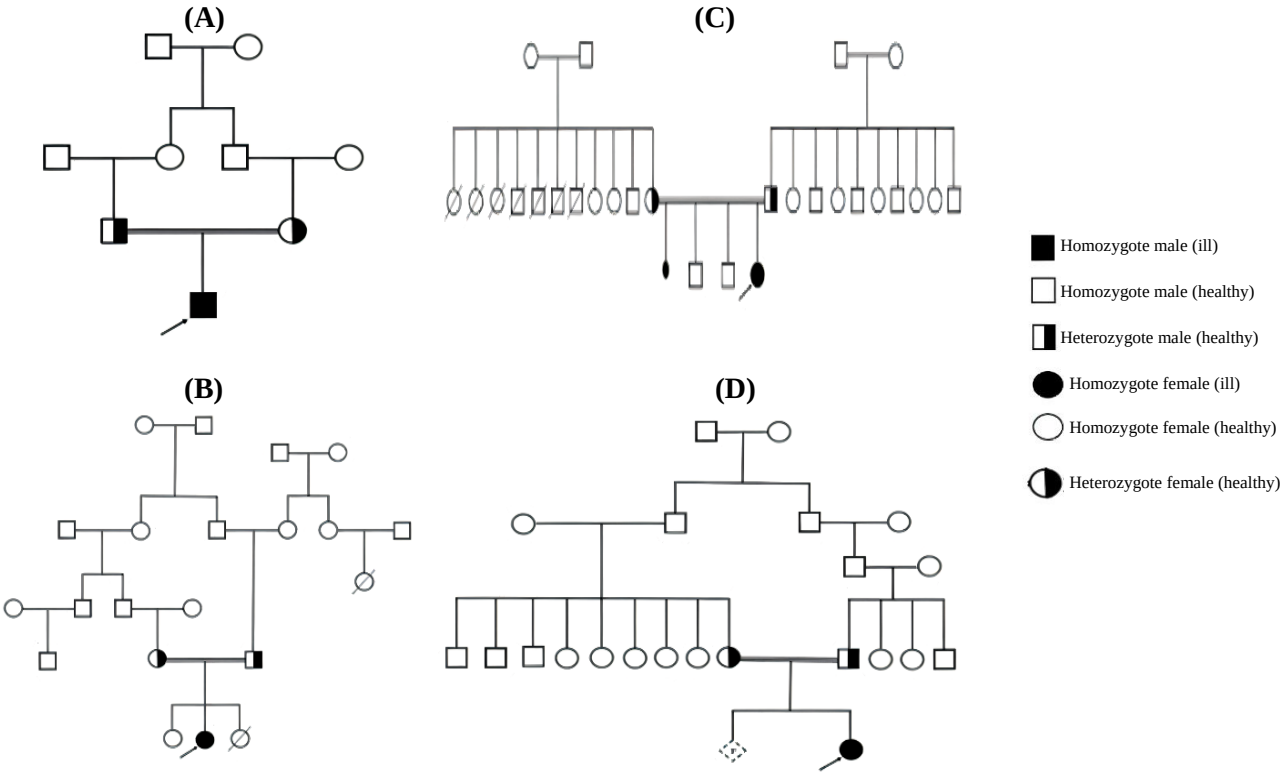

Fig. 1. Pedigrees of cohort families with recessive OI showing siblings affected by *FBBP10* mutations: (A) family 1, (B) family 2, (C) family 3, and (D) family 4.

[DOI: 10.61882/ibj.5278]

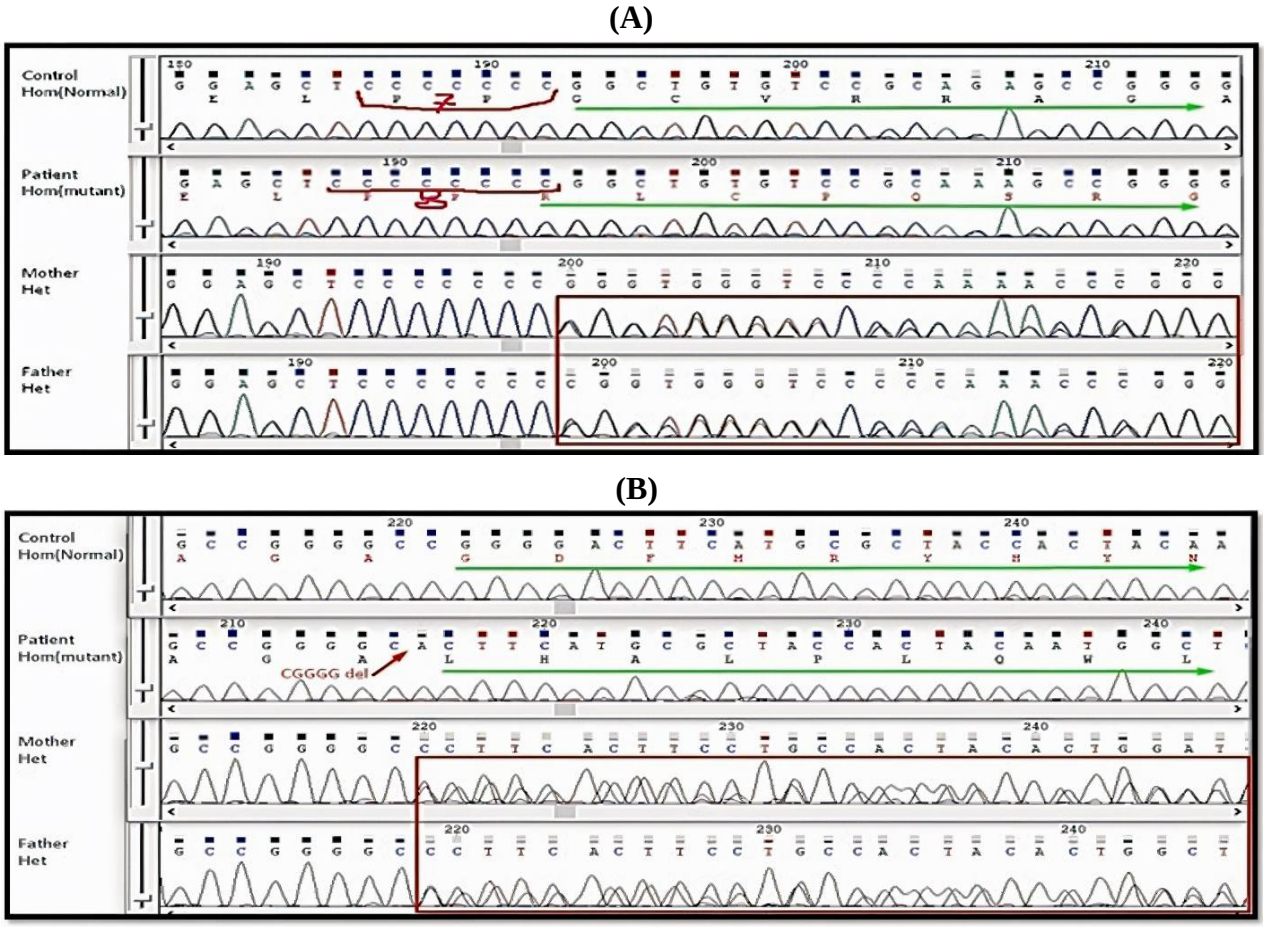

Fig. 2. Sanger sequencing chromatograms. Sequencing confirmed homozygous mutations—(A) NM_021939.3: exon5, c.831dupC (p.G278Rfs*95); (B) NM_021939: exon5, c.855_859del (p.G286Lfs*84)—in patients. Parents were heterozygous carriers, consistent with an autosomal recessive inheritance pattern.

(NM_021939.3: exon5: c.831dupC: p. G278Rfs*95). Their parents were confirmed to be heterozygous carriers of this mutation. This variant, located in exon 5 of the gene on chromosome 17q21.2 (genomic coordinates 41819307–41819313, GRCh38), was registered in the dbSNP database (rs137853883) and in the Osteogenesis Imperfecta Variant Database (https://databases.lovd.nl/shared/genes). For patient 3, NGS analysis identified a homozygous frameshift deletion in the *FKBP10* gene (NM_021939: exon5: c.855_859del: p. G286Lfs*84). Her parents were also confirmed as heterozygous carriers. This novel mutation, located in exon 5 at genomic coordinates 41819336–41819341 (GRCh38) on chromosome 17q21.2, was predicted to be pathogenic according to MutationTaster and CLNSIG. Importantly, it was not found in any of the significant population databases, including gnomAD (http://gnomad.broadinstitute.org/), Kaviar (http://db.systemsbiology.net/kaviar/cgi-pub/Kaviar.pl), ESP (https://vatlab.github.io/vat-docs/applications/annotation/variants/esp/), 1000 Genomes (http://www.internationalgenome.org/1000-genomes-browsers), the Osteogenesis Imperfecta Variant Database (https://databases.lovd.nl/shared/genes), and the internal Iranian exome database (BayanGene). Due to the absence of prior reports, this mutation is considered novel.

PCR amplification and sanger sequencing results

Targeted PCR amplification of exon 5 of *FKBP10* produced a single, specific band of expected size (~250 bp) (Fig. S1) in all patient samples, indicating successful amplification without non-specific products. All NGS findings were validated by sanger sequencing, which supported an autosomal recessive mode of inheritance. Sequencing chromatograms revealed nucleotide changes consistent with WES results (Fig. 2). Based on these analyses, we identified a novel frameshift mutation (NM_021939: exon5: c.855_859 del: p. G286Lfs*84) and a mutation in codon 831

[DOI: 10.61882/ibj.5278]

(NM_021939.3: exon5: c.831dupC: p. G278Rfs*95) in the *FKBP10* gene, which likely shows a potential hotspot in Iranian patients with OI.

Findings of PPI and functional enrichment analysis

According to the STRING database analysis, we identified 10 proteins functionally associated with *FKBP10*, which aligns with a previous report[26]. These proteins included ELN, PPIB, KDELR3, SERPINH1, LEPRE1, HSP90AA1, SERPINF1, IFITM5, PLOD2, and CRTAP. STRING provides comprehensive information on both known and predicted PPIs, encompassing direct physical contacts as well as indirect functional associations. To further explore the biological relevance of these interactions, we performed functional enrichment analysis using ClueGO v. 2.5.8[28]. This analysis revealed that the *CRTAP*, *IFITM5*, *SERPINF1*, *PPIB*, *FKBP10*, *P3H1*, *SERPINH1*, and *PLOD2* genes are significantly involved in key biological pathways and gene ontology ($p < 0.05$; Table S1). In the interaction network, the first-neighbor nodes of *FKBP10* were enriched in pathways such as type I collagen synthesis in the context of OI, the OI disease pathway, and biological processes, including collagen fibril organization, protein hydroxylation, and peptidyl-proline modification (Fig. 3). The bioinformatics analysis in our study examined the role of the PPIase protein encoded by the *FKBP10* gene in the pathways of collagen biosynthesis, fibril organization, folding, PTM modification of collagen, and OI pathogenesis. The findings highlight the central role of the *FKBP10* gene in the construction of the extracellular matrix and skeletal development. Therefore, the novel and previously reported frameshift mutations identified in our study, resulted in the synthesis of truncated FKPB65 proteins. These mutant proteins could destroy collagen—the critical and predominant protein in the bone matrix—due to their inability to induce proper folding and PTMs of collagen.

In silico predictions of the functional impact of FKBP10 mutations

Based on the protein domain analysis tool InterProScan, FKBP10 (a 64.2 kDa protein with 582 amino acids) consists of four PPIase domains and two EF-hand domains, which serve as calcium-binding sites. InterProScan results showed that both mutant proteins had a partial loss of PPIase 3 at the C-terminal and a complete loss of PPIase 4. Additionally, both calcium-binding sites (EF-hands) were removed, which could have a significant adverse effect on the biological activity of the mutants (Fig. 4). The three-dimensional structure of FKBP10 was investigated using modeling tools, such as Modeller, Swiss-Model, and AlphaFold. The Swiss-Model template covered 85% of the target protein with an identity score of 48%. The Modeler combined two templates, each covering 24% and 22% of the target protein, to produce a hybrid model covering 78% of the target protein. AlphaFold predicted a structure without template constraints, which exhibited

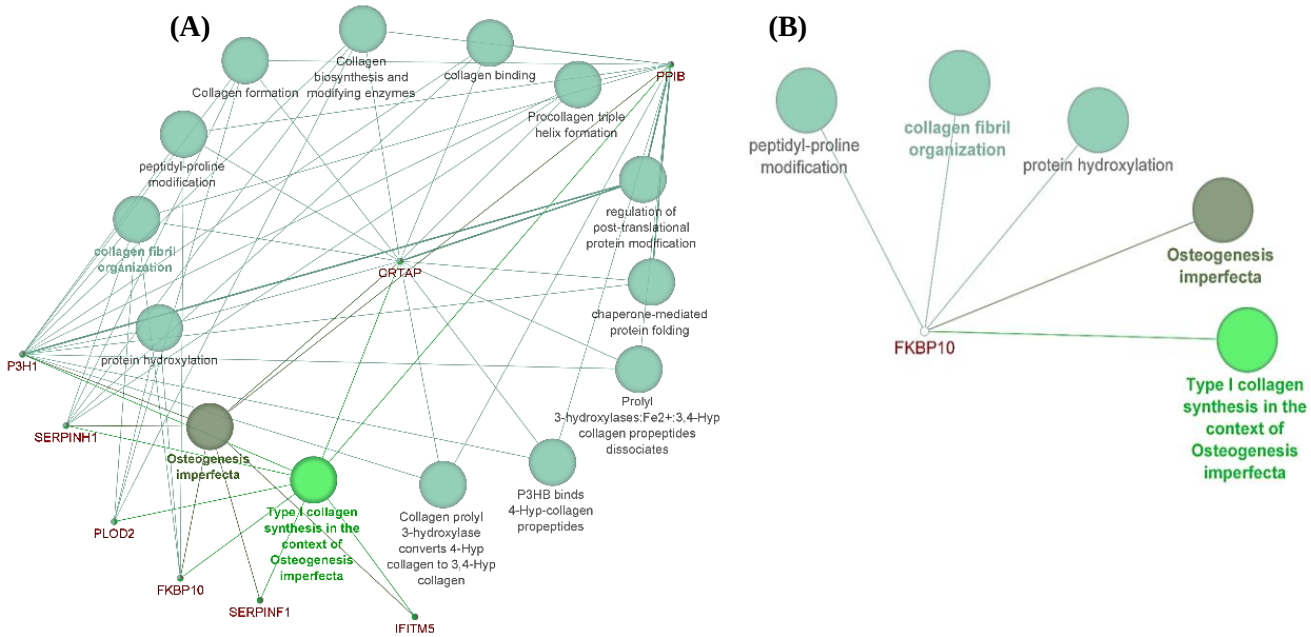

Fig. 3. PPI network of *FKBP10*. (A) STRING–based PPI network illustrating interactions between FKBP10 and proteins involved in biological pathways, such as collagen PTM and OI; (B) the network indicating the central role of FKBP10 in collagen biology and highlighting its crucial contribution to skeletal integrity.

[DOI: 10.61882/ibj.5278]

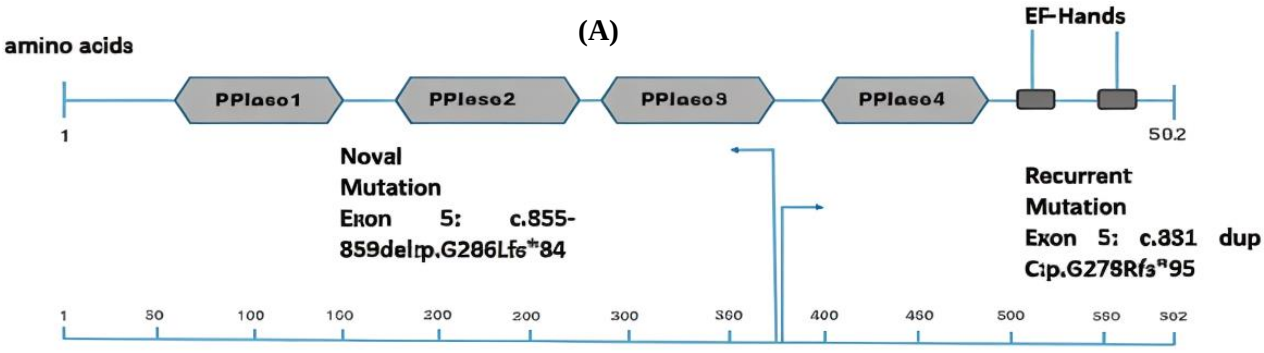

(B)

Domain Name	Start Position	End Position
PPIase 1	62	150
PPIase 2	174	262
PPIase 3	286	374
PPIase 4	399	486
EF-hand1	505	525
EF-hand 2	548	568

Fig. 4. Domain architecture analysis of the FKBP10 protein and the effect of frameshift mutations. (A) Domain architecture of the FKBP10 protein (582 amino acids) and the impact of frameshift mutations. FKBP10 belongs to the PPIase superfamily, which catalyzes the cis-trans isomerization of proline bonds, a crucial step in protein folding. The FKBP10 protein contains four PPIase domains and two EF-hand calcium-binding motifs, which are predicted toparticipate in structural stabilization and collagen folding regulaby InterProScan. The frameshift mutations identified in this study (p.G278Rfs*95 (373 amino acids) and p.G286Lfs*84 (370 amino acids) map to exon 5, resulting in truncated proteins with partial loss of PPIase 3, complete loss of PPIase 4, and deletion of both EF-hand motifs; (B) the positions of FKBP10 domains with their start and end positions.

91.5% coverage and the least structural deviation. According to Ramachandran plot analysis, both the native and mutant *FKBP10* models revealed acceptable regions in the allowed and favored conformations. However, a small number of residues were observed outside the ideal distribution, primarily located in the plot's peripheral areas. Notably, the AlphaFold predicted model exhibited the lowest deviation and the highest proportion of residues within the allowed regions, suggesting superior accuracy (Fig. S2). We submitted the three models to the PROCHECK server for further evaluation. Based on our results, the AlphaFold model achieved the highest overall quality and structural correctness scores, followed by Modeller and Swiss-Model. Notably, AlphaFold predicted fewer incorrect residues and more correctly predicted secondary structure elements. These findings demonstrate that among the three software tools tested, AlphaFold generated the most accurate model of the FKBP10 protein (Fig. 5), which aligns with recent comparative studies ranking AlphaFold among the most reliable homology modeling algorithms[35].

MD simulation

The MD trajectory files were assessed for RMSD, RMSF, Rg, and SASA, as shown in Figure 6. RMSD was used to assess deviations between the final and initial atomic positions of the protein[32]. The results indicated that mutant 1 of *FKBP10* (G286Lfs*84) exhibited lower fluctuations over a 100 ns simulation than either the *FKBP10* wild-type or mutant 2. Average RMSD values during the last 20 ns were 0.87 ± 0.08 nm for wild-type, 0.88 ± 0.05 nm for p.G286Lfs*84, and 1.02 ± 0.04 nm for p.G278Rfs*95 (Table 2), with equilibration time reached at ~80 ns. RMSF analysis showed higher residue-level fluctuations in wild-type FKBP10 (mean 0.45 ± 0.16 nm), as compared to both G286Lfs*84 (mean 0.28 ± 0.18 nm) and G278Rfs*95 (mean 0.34 ± 0.23 nm) mutants, suggesting greater conformational flexibility in the wild-type protein. Notably, RMSF values at the mutated residue 286 (variants G286Lfs*84) and residue 278 (variants G278Rfs*95) increased by ~2-3-fold. Rg analysis over a 100 ns simulation depicted that the wild-type FKBP10 model maintained an expanded and relatively stable conformation, with Rg values averaging 4.97 ± 0.06 nm. In contrast, the mutant variants G286Lfs*84 (mean 3.07 ± 0.04 nm) and G278Rfs*95 (mean 3.08 ± 0.00 nm) showed lower Rg values and reduced fluctuations.

[DOI: 10.61882/ibj.5278]

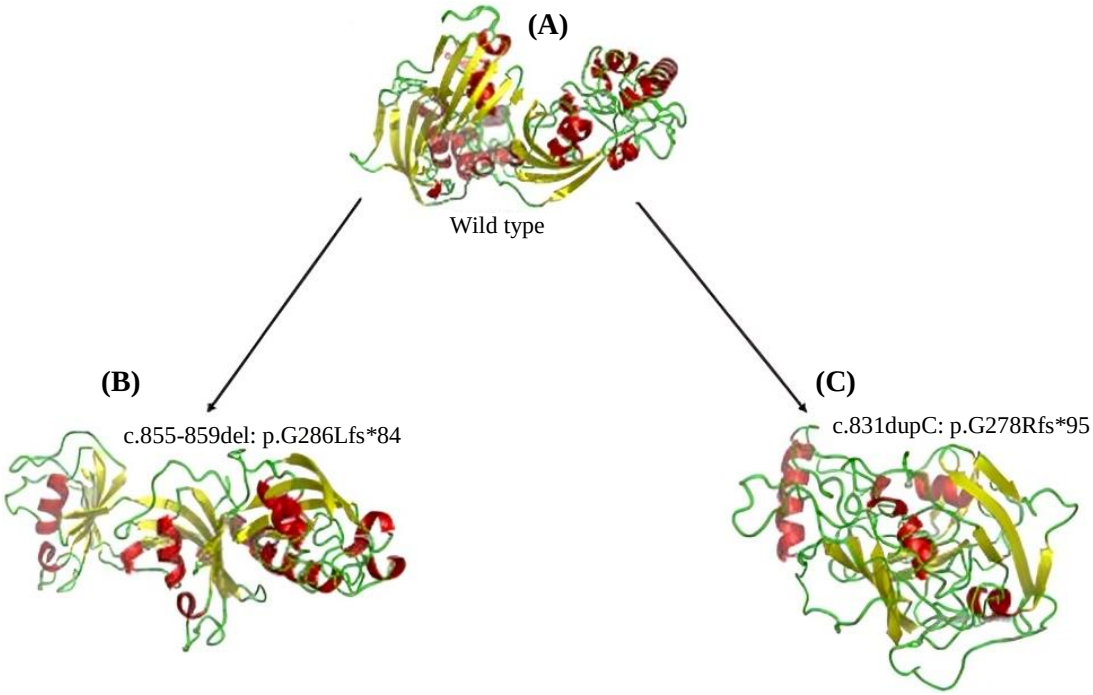

Fig. 5. Homology modeling of the FKBP10 protein. (A Predicted three-dimensional (3D) structure of the wild-type FKBP10 protein; (B) predicted 3D structure of the truncated protein (p.G286Lfs*84), lacking part of the PPIase domain and EF-hand Ca-binding motif; (C) predicted 3D structure of the mutant protein (p.G278Rfs*95), a shortened FKBP10 protein with disrupted domain organization. Models generated by homology modeling revealed structural destabilization and domain loss in frameshift variants compared to the wild-type protein. red, yellow, and green show α-helices, β-sheets, and loops, respectively.

The SASA graph compares the SASA of FKBP10 wild-type and two frameshift mutant proteins (G286Lfs*84 and G278Rfs*95) over a 100-ns simulation. The higher and more stable SASA in FKBP10, with a mean of 327.55 ± 3.72 nm, characterized the wild-type protein. RMSD was used to assess deviations in the final and initial atomic positions of the protein.

DISCUSSION

The current study identified two mutations in exon 5 of the *FKBP10* gene through WES, a recurrent frameshift insertion (c.831dupC; p.G278Rfs*95) and a novel homozygous deletion (c.855_859 del; p.G286Lfs*84). Both mutations were confirmed by targeted PCR and sanger sequencing. To our knowledge, this is the first cohort study to report *FKBP10* mutation screening in OI from Iran, and the first worldwide description of the novel mutation. The c.831dupC mutation in exon 5 of *FKBP10* has been widely recognized as a mutational hotspot due to its high frequency, recurrence across diverse unrelated populations, and frequent reporting in the literature[11,12,16,36,37]. The presence of mononucleotide repeats (poly-C) at this site predisposes it to polymerase slippage and recurrent insertions. This condition increases the likelihood of mutation occurrence[12]. However, in African populations, , the recurrence of this mutation has been linked to a founder effect, in which a single ancestral mutation becomes frequent through inheritance rather than site instability[38].

The identified mutations were classified as pathogenic according to the ACMG/AMP 2015 guidelines[39]. Frameshift mutations with premature stop codons produced truncated proteins and strongly met the PVS1 criteria (loss of function). Additional criteria included PM2 (absence from population databases), PP1 (homozygosity in affected patients and heterozygosity in parents, referring to the recessive inheritance pattern), PP3 (computational in silico prediction of domain loss using InterProScan and molecular simulations), and PP4 (phenotypic specificity, including early-onset fractures and bone fragility characteristics of OI type XI). The justification for each criterion are detailed in Table S2.

In the present study, bioinformatics analysis indicated that *FKBP10* plays a crucial role in collagen and elastin processing and serves as a key component of the complex protein network within the extracellular matrix[9,40]. Network and enrichment analyses revealed associations between *FKBP10* and genes such as

[DOI: 10.61882/ibj.5278]

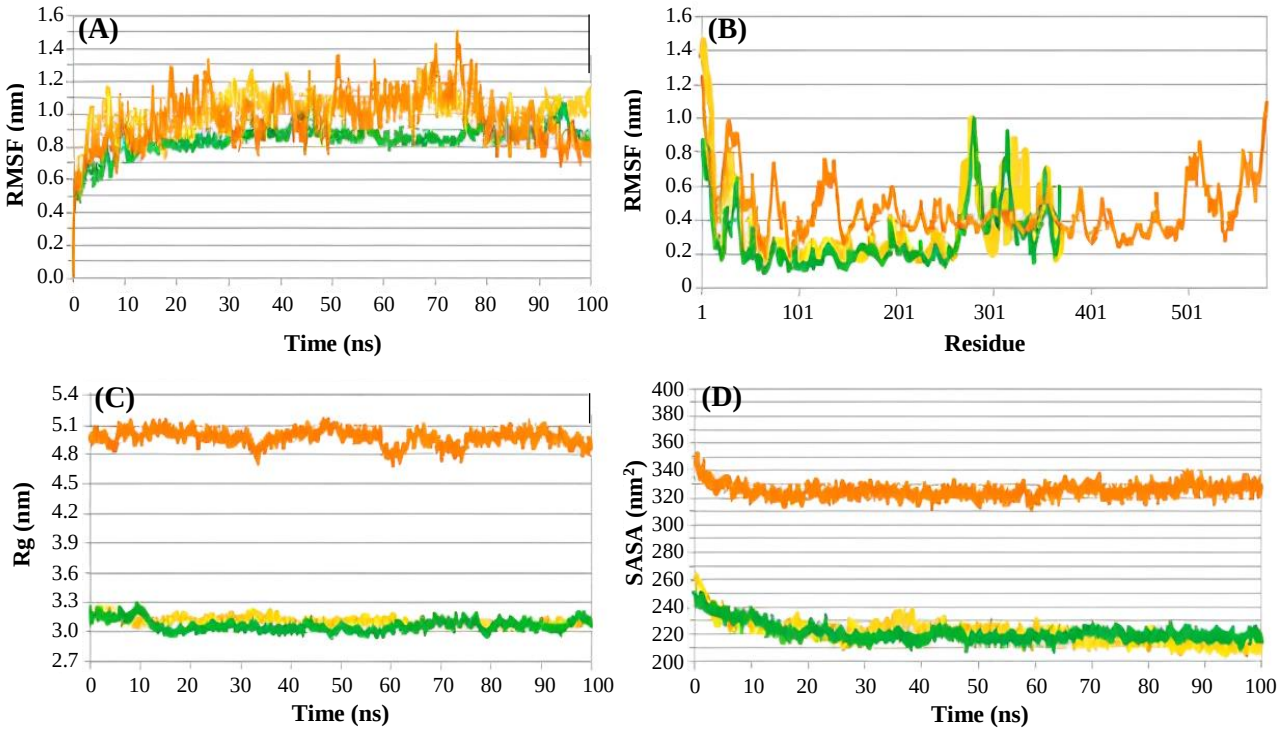

Fig. 6. Structural dynamics of the FKBP10 protein (wild-type) and mutants. (A) RMSD, (B) RMSF, (C) radius of MD dynamics simulation. Orange indicates the FKBP10 wild-type, while green and yellow represent the frameshift mutant proteins p.G286Lfs*84 and p.G278Rfs*95, respectively. RMSD and RMSF reflect structural stability and flexibility, Rg depicts protein compactness, and SASA indicates solvent exposure differences between wild-type and mutant types.

CRTAP, *P3H1*, *SERPINH1*, *PLOD2*, *SERPINF1*, *PPIB*, and *IFITM1* across several biological pathways, including collagen fibril organization, hydroxylation, folding, and cross-linking. In line with previous reports, disruption of *FKBP10* activity destabilizes collagen fibrils, leading to a disorganized bone matrix and the OI phenotype[9,40]. These findings support previous reports that FKBP10 does not function as an isolated chaperone but as a component of a larger ER chaperone complex, which is essential for collagen type I folding and modification[9,40]. The findings further emphasize the role of FKBP10 in stabilizing the collagen helix via its PPIase activity. Moreover, grouping *FKBP10*, *SERPINH1*, and *CRTAP* as responsible genes for recessive OI with similar phenotypes supports the concept of "chaperon disease" or "chaperoneopathy"[41].

Domain architecture analysis using UniProt and InterProScan (an in silico prediction tool) revealed that the frameshift mutations truncate the wild-type FKBP10 protein (582 amino acids), producing the variants p.G278Rfs95 and p.G286Lfs84, which consist of 373 and 370 amino acids, respectively. Both variants indicated the complete loss of the PPIase4 domain (residues 399-486) and partial deletion of PPIase3 at the C-terminal. These alterations disrupt PPIase activity and impair collagen folding. Furthermore, the two EF-hand calcium-binding motifs (residues 505-568) and the C-terminal HEEL motif (close to residue 580) were destroyed in both truncated proteins. These domains contribute to protein stability via calcium binding and ER retention, respectively. Consequently, the loss of the mentioned domains impairs the structure and function of the FKBP10 protein, which is consistent with previously reported data[12,42].

Table 2. Average structural parameters predicted by MD simulations

Complex	Mean RMSD (nm)	Mean RMSF (nm)	Mean Rg (nm)	Mean SASA (nm)
FKBP10 (Wild Type)	0.87 ± 0.08	0.45 ± 0.16	4.97 ± 0.06	327.55 ± 3.72
Mutant 1 (p. G286Lfs*84)	0.88 ± 0.05	0.28 ± 0.18	3.07 ± 0.04	218.73 ± 2.48
Mutant 2 (p. G278Rfs*95)	1.02 ± 0.04	0.34 ± 0.23	3.08 ± 0.00	212.52 ± 3.33

[DOI: 10.61882/ibj.5278]

MD simulations revealed lower RMSF values in mutant proteins compared to wild-type, indicating a more dynamic and flexible conformation in the original protein. However, decreases in Rg and SASA values, together with reduced intramolecular hydrogen bonding, supported the presence of more compact and conformationally constrained mutant structures. Proteins exhibiting these features—greater rigidity, diminished flexibility, and compromised cohesiveness—tend to adopt destabilized conformations. Such structural alterations are likely to impair biological activity or promote the pathogenic potential of mutant proteins by disrupting the native functional dynamics of wild-type FKBP10. In light of these findings, frameshift mutations were determined to produce truncated FKBP10 proteins characterized by poor stability, inefficient folding, and impaired interactions with collagen[32,43].

FKBP10 mutations are also responsible for Bruck syndrome type I, while *PLOD2* mutations cause type II[10,36,44]. According to the literature, the c.831dupC mutation has been reported to contribute to Bruck syndrome and OI, even within the same family[10,12,14]. STRING database analysis identified *FKBP10* and *PLOD2* as connected genes, and ClueGO functional analysis revealed shared gene ontology and pathways[16,45].

Interestingly, Kaneto et al. reported that in a Bruck syndrome patient with the *FKBP10* c.831dupC mutation, osteogenesis-related gene expression differed from that in OI patients and more closely resembled healthy controls. They proposed that such distinct expression patterns may reflect differences in downstream transcriptional regulatory mechanisms contributing to the divergent BRUCK syndrome versus OI phenotype[46]. Consistent with this study and despite the involvement of *FKBP10* and *PLOD2* in similar molecular networks, the *FKBP10* c.831dupC variant and absence of joint contractures in our patients supported a diagnosis of OI rather than Bruck syndrome. These observations highlight that *FKBP10* variants alone are insufficient to determine whether the clinical outcome is for OI or Bruck syndrome. Instead, the final phenotype likely results from a combination of factors, including complex genotype–phenotype relationships, differential downstream transcriptional regulation, additional modifier genes, and possibly environmental influences, which warrant further analytical investigation[12,14].

Clinically, all affected individuals in our cohort carried homozygous mutations, while their parents were heterozygous carriers, corroborating the autosomal recessive inheritance of *FKBP10*-related OI. As reported in the literature, *FKBP10*-related OI is typically associated with biallelic pathogenic variants (homozygous or compound heterozygous) in affected individuals. However, heterozygous carriers are often unaffected. Accordingly, consanguinity increases the likelihood of homozygous pathogenic variants in such genes. The association of consanguinity with homozygous mutations in our cohort, which are consistent with previous studies, highlights the impact of population genetics on OI incidence[11,17]. These findings further highlight the importance of carrier screening and genetic counseling in regions with high rates of consanguinity and endogamy[37,47].

Phenotypic heterogeneity among our patients reflects the complexity of genotype-phenotype correlations observed in *COL1A1*, *COL1A2*[48], and other recessive OI genes[49,50]. Such variability may be influenced by factors such as mutation type (missense, frameshift, and nonsense), the extent of protein truncation (depending on mutation position), degree of loss of function, residual enzyme activity[50], disruption of collagen cross-linking, and the presence of modifier genes[9,36].

In this study, the relatively small sample size (30 families) reflects both the rarity of OI and the single-center design, which could be considered a limitation. Furthermore, MD and modeling predictions were not validated experimentally in vitro. Therefore, the structural effects should be interpreted as mechanistic hypotheses generated by computational analysis rather than definitive functional impairments. Nevertheless, integrating WES, structural modeling, and MD simulations provided the first mechanistic insights into FKBP10 dysfunction in OI. Larger, multicenter studies incorporating in vitro functional validations are warranted to strengthen and extend these observations.

CONCLUSION

This study reports the first identification of *FKBP10* mutations in a cohort of 30 Iranian patients with OI. The mutations included a novel homozygous frameshift (c.855_859del; p.G286Lfs*84), not previously described worldwide, and the recurrent c.831dupC; p.G278Rfs95 variant. Our findings expand the *FKBP10* mutational spectrum and propose c.831dupC in exon 5 of *FKBP10* as a potential hotspot. The present study is the first to explore the structural and dynamical features of *FKBP10* variants by integrating WES, PPI network analysis, and MD simulations, thereby linking genotype to FKBP10 protein function. Computational analyses predicted that frameshift mutations destabilize protein conformation and enhance the pathogenic potential of FKBP10 mutants. Our findings highlight the importance of population-based genetic studies, particularly in

[DOI: 10.61882/ibj.5278]

regions with high rates of consanguinity and predisposition to recessive OI. Early identification of such mutations enables timely clinical interventions, reduces disease burden, and facilitates informed family planning. Future investigations should validate these computational predictions experimentally and extend genetic analyses to larger cohorts to support the development of improved diagnostic and therapeutic approaches.

DECLARATIONS

Acknowledgments

In providing this manuscript, we have used Grammarly for language corrections. The AI photo enhancer, cutout.pro (https://www.cutout.pro/photo-enhancer-sharpener-upscaler/upload) has been applied to improve the quality of the figures.

Ethical approval

All experiments were performed in accordance with relevant guidelines and regulations of the Ethics Committee, at the Pasteur Institute of Iran (ethical approval code: IR.Pii.REC.1395.107).

Consent to participate

The patients' parents signed the consent letter, permitting the use of the samples and the publication of the obtained data.

Consent for publication

All authors reviewed the results and approved the final version of the manuscript.

Authors' contributions

MH: performed the experiments and analyzed NGS data; SM: performed the experiments, did bioinformatics, in silico analysis, protein modeling, and analyzed NGS data; FM: performed the experiments; FSS: assisted the MD analysis, analyzed the final data and drafted the manuscript; PE: designed the study; MRA: clinically diagnosed the patients with OI, identified the clinical type of the disease, and referred them to the Biochemistry Department of the Pasteur Institute of Iran; MER: designed the study, did bioinformatics, in silico analysis, protein modeling, MD simulations, analyzed the final data, and drafted the manuscript.

Data availability

All relevant data supporting the study's findings are presented within the manuscript and supplementary file. Additional data or answers to the questions may be provided upon request.

Competing interests

The authors declare that they have no competing interests.

Funding

This study was supported by a research grant from the Pasteur Institute of Iran.

Supplementary information

The online version contains the supplementary material.

REFERENCE

1. Mujanovic N. Osteogenesis imperfecta-a current overview. Surg Child. 2025;2(1):28-32.
2. Lin X, Hu J, Zhou B, Zhang Q, Jiang Y, Wang O, et al. Genotype–phenotype relationship and comparison between eastern and western patients with osteogenesis imperfecta. J Endocrinol Invest. 2024;47(1):67-77.
3. Sillence DO. A dyadic nosology for osteogenesis imperfecta and bone fragility syndromes 2024. Calcif Tissue Int. 2024;115(6):873-90.
4. Batkovskyte D, Swolin-Eide D, Hammarsjö A, Sæther KB, Thunström S, Lundin J, et al. Structural variants in COL1A1 and COL1A2 in osteogenesis imperfecta. Am J Med Genet A. 2025;197(3):63935.
5. Valadares ER, Carneiro TB, Santos PM, Oliveira AC, Zabel B. What is new in genetics and osteogenesis imperfecta classification? J Pediatr. 2014;90(6):536-41.
6. Sillence D. AB019. Osteogenesis imperfecta 2015: New genes, new treatments—an Asia pacific perspective. Ann Transl Med. 2015;3(2):19.
7. Patterson CE, Gao J, Rooney AP, Davis EC. Genomic organization of mouse and human 65 kDa FK506-binding protein genes and evolution of the FKBP multigene family. Genomics. 2002;79(6):881-9.
8. Murphy LA, Ramirez EA, Trinh VT, Herman AM, Anderson VC, Brewster JL. Endoplasmic reticulum stress or mutation of an EF-hand $Ca(2^{+})$-binding domain directs the FKBP65 rotamase to an ERAD-based proteolysis. Cell Stress Chaperones. 2011;16(6):607-19.
9. Barnes AM, Cabral WA, Weis M, Makareeva E, Mertz EL, Leikin S, et al. Absence of FKBP10 in recessive type XI osteogenesis imperfecta leads to diminished collagen cross-linking and reduced collagen deposition in extracellular matrix. Hum Mutat. 2012;33(11):1589-98.
10. Otaify GA, Abdel-Hamid MS, Hassib NF, Elhossini RM, Abdel-Ghafar SF, Aglan MS. Bruck syndrome in 13 new patients: Identification of five novel FKBP10 and PLOD2 variants and further expansion of the phenotypic spectrum. Am J Med Genet A. 2022;188(6):1815-25.
11. Alanay Y, Avaygan H, Camacho N, Utine GE, Boduroglu K, Aktas D, et al. Mutations in the gene encoding the RER protein FKBP65 cause autosomal-recessive osteogenesis imperfecta. Am J Hum Genet. 2010;86(4):551-9.
12. Merkuryeva ES, Markova TV, Kenis VM, Agranovich

[DOI: 10.61882/ibj.5278]

OE, Dan IM, Kotalevskaya YY, et al. Presentation of rare phenotypes associated with the FKBP10 gene. Genes. 2024;15(6):674.
13. Alfares A, Alfadhel M, Wani T, Alsahli S, Alluhaydan I, Al Mutairi F, et al. A multicenter clinical exome study in unselected cohorts from a consanguineous population of Saudi Arabia demonstrated a high diagnostic yield. Mol Genet Metab. 2017;121(2):91-5.
14. Essawi OH, Tapaneeyaphan P, Symoens S, Gistelinck C, Malfait F, Eyre DR, et al. New insights on the clinical variability of FKBP10 mutations. Eur J Med Genet. 2020;63(9):103980.
15. Chetty M, Roberts T, Shaik S, Beighton P. Dentinogenesis imperfecta in osteogenesis imperfecta type XI in South Africa: A genotype–phenotype correlation. BDJ Open. 2019;5(1):4.
16. Shaheen R, Al-Owain M, Faqeih E, Al-Hashmi N, Awaji A, Al-Zayed Z, et al. Mutations in FKBP10 cause both bruck syndrome and isolated osteogenesis imperfecta in humans. Am J Med Genet A. 2011;155(6):1448-52.
17. Seyedhassani SM, Hashemi-Gorji F, Yavari M, Harazi F, Yassaee VR. Novel FKBP10 mutation in a patient with osteogenesis imperfecta type XI. Fetal Pediatr Pathol. 2016;35(5):353-8.
18. Evin F, Atik T, Onay H, Goksen D, Darcan S, Cogulu O, et al. Effectiveness of whole exome sequencing analyses in the molecular diagnosis of osteogenesis imperfecta. J Pediatr Endocrinol Metab. 2024;37(8):693-700.
19. Childers MC, Daggett V. Insights from molecular dynamics simulations for computational protein design. Mol Syst Des Eng. 2017;2(1):9-33.
20. Huang J, Liang X, Xuan Y, Geng C, Li Y, Lu H, et al. A reference human genome dataset of the BGISEQ-500 sequencer. Gigascience. 2017;6(5):1-9.
21. Li H, Durbin R. Fast and accurate short read alignment with Burrows–Wheeler transform. Bioinformatics. 2009;25(14):1754-60.
22. McKenna A, Hanna M, Banks E, Sivachenko A, Cibulskis K, Kernytsky A, et al. The genome analysis toolkit: A mapreduce framework for analyzing next-generation DNA sequencing data. Genome Res. 2010;20(9):1297-303.
23. Karczewski KJ, Francioli LC, Tiao G, Cummings BB, Alföldi J, Wang Q, et al. The mutational constraint spectrum quantified from variation in 141,456 humans. Nature. 2020;581(7809):434-43.
24. Auton A, Salcedo T. The 1000 genomes project. Assessing rare variation in complex traits; Design and analysis of genetic studies. Springer. 2015:71-85.
25. Lek M, Karczewski KJ, Minikel EV, Samocha KE, Banks E, Fennell T, et al. Analysis of protein-coding genetic variation in 60,706 humans. Nature. 2016;536(7616):285-91.
26. Szklarczyk D, Gable AL, Nastou KC, Lyon D, Kirsch R, Pyysalo S, et al. The STRING database in 2021: Customizable protein–protein networks, and functional characterization of user-uploaded gene/measurement sets. Nucleic Acids Res. 2021;49(1):605-12.
27. Shannon P, Markiel A, Ozier O, Baliga NS, Wang JT, Ramage D, et al. Cytoscape: A software environment for integrated models of biomolecular interaction networks. Genome Res. 2003;13(11):2498-504.
28. Bindea G, Mlecnik B, Hackl H, Charoentong P, Tosolini M, Kirilovsky A, et al. ClueGO: A cytoscape plug-in to decipher functionally grouped gene ontology and pathway annotation networks. Bioinformatics. 2009;25(8):1091-3.
29. Bordoli L, Kiefer F, Arnold K, Benkert P, Battey J, Schwede T. Protein structure homology modeling using SWISS-MODEL workspace. Nat Protoc. 2009;4(1):1-13.
30. Das S, Johri P, Sharma R, Kashyap M, Singh S, Singh S. Comparative modeling, characterization and energy minimization studies of aquaporin 9: An exclusive target protein for rheumatoid arthritis. Int J Pharm Investig. 2019;9(2):43-6.
31. Blum M, Chang H-Y, Chuguransky S, Grego T, Kandasaamy S, Mitchell A, et al. The interPro protein families and domains database: 20 years on. Nucleic Acids Res. 2021;49(1):344-54.
32. Aris P, Mohamadzadeh M, Wei Y, Xia X. In Silico molecular dynamics of griseofulvin and its derivatives revealed potential therapeutic applications for COVID-19. Int J Mol Sci. 2022;23(13):6889.
33. Hoover WG. Canonical dynamics: Equilibrium phase-space distributions. Phys Rev A Gen Phys. 1985;31(3):1695-97.
34. Essmann U, Perera L, Berkowitz ML, Darden T, Lee H, Pedersen LG. A smooth particle mesh Ewald method. J Chem phys. 1995;103(19):8577-93.
35. Kamguia SD, Njabon EN, Patouossa I, Emadak A, Forlemu N. A comparative analysis of cockroach and mosquito, octopamine receptor homologues produced using chimera, swiss-model, and alphafold molecular modeling tools. ACS Omega. 2025;10(8):7907-19.
36. Kelley BP, Malfait F, Bonafe L, Baldridge D, Homan E, Symoens S, et al. Mutations in FKBP10 cause recessive osteogenesis imperfecta and Bruck syndrome. J Bone Miner Res. 2011;26(3):666-72.
37. Caparros-Martin JA, Aglan MS, Temtamy S, Otaify GA, Valencia M, Nevado J, et al. Molecular spectrum and differential diagnosis in patients referred with sporadic or autosomal recessive osteogenesis imperfecta. Mol Genet Genomic Med. 2016;5(1):28-39.
38. Vorster A, Beighton P, Chetty M, Ganie Y, Henderson B, Honey E, et al. Osteogenesis imperfecta type 3 in South Africa: Causative mutations in FKBP10. S Afr Med J. 2017;107(5):457-62.
39. Richards S, Aziz N, Bale S, Bick D, Das S, Gastier-Foster J, et al. Standards and guidelines for the interpretation of sequence variants: A joint consensus recommendation of the American college of medical genetics and genomics and the association for molecular pathology. Genet Med. 2015;17(5):405-24.
40. Duran I, Martin JH, Weis MA, Krejci P, Konik P, Li B, et al. A chaperone complex formed by HSP47, FKBP65, and BiP modulates telopeptide lysyl hydroxylation of type I procollagen. J Bone Miner Res. 2017;32(6):1309-19.
41. Claeys L, Storoni S, Eekhoff M, Elting M, Wisse L, Pals G, et al. Collagen transport and related pathways in

[DOI: 10.61882/ibj.5278]

osteogenesis imperfecta. Hum Genet. 2021;140(8):1121-41.
42. Steinlein OK, Aichinger E, Trucks H, Sander T. Mutations in FKBP10 can cause a severe form of isolated osteogenesis imperfecta. BMC Med Genet. 2011;12(1):152.
43. Yao J, Ding Y, Liu X, Huang J, Zhang M, Zhang Y, et al. Application value of whole exome sequencing in screening and identifying novel mutations of hypopharyngeal cancer. Sci Rep. 2023;13(1):107.
44. Yelkur P, Mohammed S, Narayan K. Congenital contractures and fractures: A variant of Bruck syndrome type 2. Cureus. 2024;16(6):61991.
45. Puig-Hervás MT, Temtamy S, Aglan M, Valencia M, Martínez-Glez V, Ballesta-Martínez MJ, et al. Mutations in PLOD2 cause autosomal-recessive connective tissue disorders within the Bruck syndrome—osteogenesis imperfecta phenotypic spectrum. Hum Mutat. 2012;33(10):1444-9.
46. Kaneto CM, Lima PS, Zanette DL, Oliveira TYK, de Assis Pereira F, Lorenzi JCC, et al. Osteoblastic differentiation of bone marrow mesenchymal stromal cells in Bruck Syndrome. BMC Med Genet. 2016;17(1):38.
47. Sobaihi M, Habiballah AK, Habib AM. TMEM38B gene mutation associated with osteogenesis imperfecta. Cureus. 2024;16(9):69021.
48. Garibaldi N, Besio R, Dalgleish R, Villani S, Barnes AM, Marini JC, et al. Dissecting the phenotypic variability of osteogenesis imperfecta. Dis Model Mech. 2022;15(5):49398.
49. Jovanovic M, Marini JC. Update on the genetics of osteogenesis imperfecta. Calcif Tissue Int. 2024;115(6):891-914.
50. Moosa S, Yamamoto GL, Garbes L, Keupp K, Beleza-Meireles A, Moreno CA, et al. Autosomal-recessive mutations in MESD cause osteogenesis imperfecta. Am J Hum Genet. 2019;105(4):836-43.

[DOI: 10.61882/ibj.5278]